Mixing Line Analysis of Clouds and Cloudy Boundary Layers

ALAN K. BETTS*

West Pawlet, VT 05775

(Manuscript received 27 February 1985, in final form 8 July 1985)

ABSTRACT

The diagnostic study of the thermodynamic structure of nonprecipitating clouds and cloudy boundary layers is formulated using a mixing line and saturation point approach. A parametric model for the mean structure is developed as a tool for diagnostic and prognostic modeling. Cloud-scale mixing processes are analyzed in the same framework, together with the energetics of the evaporative instability in cumulus clouds. A velocity scale emerges for this evaporative instability. The statistical study of saturation level distribution in partially cloudy boundary layers is proposed to related cloud fraction to the mean thermodynamic mixing processes.

1. Introduction

This paper is an attempt to synthesize various conceptual, diagnostic, and parametric approaches to the study of both isolated clouds and cloudy boundary layers. There is a need for a general parametric model for partially mixed, partially cloudy boundary layers for incorporation in global forecast and climate simulation models. Shallow boundary layer cloud fields transport moisture away from the surface and redistribute heat in the vertical. There is a complex interaction of the mixing, condensation, evaporation and radiative processes on both the time and space scales of individual cloud elements and on the scale of the field of clouds as a whole. Cloud fields may, in addition, have mesoscale organization and the evolution of the entire cloud field is strongly controlled by the larger scale mean vertical motion field.

The use of parameters which are conserved in the liquid water to vapor phase change (Lilly, 1968; Betts, 1973, 1975; Yanai *et al.*, 1973; Ogura and Cho, 1973; Arakawa and Schubert, 1974) and in particular the use of the air parcel saturation point (Betts, 1982a,b) has proved of great value in interpreting and modeling atmospheric convective structure and transports. For nonprecipitating cloud fields the use of the saturation point, or the derived conserved parameters of equivalent potential temperature (θ_E), liquid water potential temperature (θ_L) or total water (q_T), effectively eliminates consideration of the liquid water to vapor phase change and reduces convective transports within a partially cloudy boundary layer to a simple mixing process (Betts, 1983, 1984; Hanson, 1984). This simplification (which forms the basis for this paper) permits the parameterization of shallow cloud fields in global models in terms of a mixing line process (Betts and Miller, 1984). Conserved parameter methods have also been useful in the study of the transition between stratocumulus and broken cumulus associated with the cloud top entrainment instability (Lilly, 1968; Randall, 1980; Deardorff, 1980; Moeng and Arakawa, 1980) although this transition is not yet fully understood (Hanson, 1984; Randall, 1984). It is this instability that makes shallow cumulus fields an inherently destabilizing mechanism in the atmosphere (Betts, 1973), and promotes cloud-top entrainment (Squires, 1958; Paluch, 1979) within individual clouds, while the circulations within a stratocumulus layer are more dependent on radiative processes at cloud top (Lilly, 1968; Schubert, 1976; Deardorff, 1976, 1981; Kahn and Businger, 1981a,b). One consequence is that cumulus layers are not as well mixed as stratocumulus layers.

Global models need to parameterize all types of shallow cloud fields (Suarez *et al.*, 1983). Their vertical transports of heat and moisture control the surface latent and sensible heat fluxes, and hence the long-term mean precipitation. Without a shallow cloud parameterization to transport water vapor out of the subcloud layer, the surface latent heat flux is underestimated, global precipitation is reduced, and a global model climate drifts toward lower temperatures, particularly in the tropics (Betts and Miller, 1984). Well-mixed boundary layer parameterizations have been proposed for global models (Deardorff, 1972; Arakawa and Schubert, 1974; Suarez *et al.*, 1983), sometimes in conjunction with a separate parameterization for cumulus clouds (Arakawa and Schubert, 1974). The philosophy behind this paper is to develop a cloudy boundary layer parameterization with a common

* Visiting Scientist, Goddard Space Flight Center, Code 613, MD 20771.

structure for cumulus and stratocumulus, in which a parameter is introduced to represent how well mixed the layer is in the vertical. A theoretical framework for the diagnostic study of cloudy boundary layers is needed since improvements in parametric modeling need observational statistics on mean boundary layer structure and variance over a wide range of types of cloud fields. We shall not address, in this paper, the prediction of boundary layer depth in a large-scale model since diagnostically this is an observable characteristic.

We shall first consider a parametric idealization of the thermodynamic structure of a partially mixed boundary layer using a conserved parameter mixing line method (Betts, 1982a,b), and then explore cloud-scale mixing and the energetics of evaporative entrainment instability. Finally, we discuss the relationship between the saturation level distribution and fractional cloudiness.

2. Saturation point framework

The saturation point (SP) framework is discussed in a series of papers (Betts, 1982a,b; 1983; 1984). In essence, the SP of an air parcel is found by dry (moist) adiabatic ascent (descent) to the pressure level (p^*) where a parcel is just saturated (with no cloud liquid water). At this saturation level (SL) parcel temperature and pressure (T^*, p^*) uniquely specify the conserved thermodynamic parameters (θ_E, θ_L, and q_T) which are invariant for both dry and moist adiabatic processes and approximately conserved in isobaric mixing processes. When two air parcels mix, the SP of every possible mixture lies on a mixing line joining the SPs of the two parcels (Betts, 1982a). In this conserved parameter framework a shallow cloud field can be regarded as a mixing process between the surface superadiabatic layer and the free atmosphere, and the process can be characterized by a mixing line. In fact, in boundary layers in convective–radiative equilibrium, radiative processes can produce measurable deviations from a mixing line structure (Betts, 1982a; 1983). A later paper will discuss convective–radiative equilibrium and attempt to quantify nonequilibrium departures from a mixing line structure. For the purposes of this largely theoretical paper, we shall regard the mixing line model as a useful idealization.

One advantage of the SP framework is that virtual potential temperatures can be computed for unsaturated and cloudy air parcels (Betts, 1982a, 1983). For brevity, we shall call the isopleths joining SPs of equal virtual temperature for unsaturated and cloudy air parcels (Γ_{vu} and Γ_{vc}, respectively) the *dry virtual adiabat* and the *moist virtual adiabat,* since these replace the dry and moist adiabats in analyses of buoyancy. The slopes of the mixing line and these virtual adiabats will be linearized for analytic purposes, although for data analysis this is not necessary since both mixing line and data can be plotted directly on a thermodynamic diagram.

3. Parametric structure for layer

This section introduces an idealized mixing line model characterized by a mixing line slope and the distribution of saturation level with pressure. These parameters are then used to discuss cloud layer structure and cloud-top entrainment instability.

a. Idealized mixing line (ML) model

Figure 1 shows an idealized conceptual model for the equilibrium thermodynamic structure of a partially cloudy boundary layer drawn on a schematic thermodynamic diagram, in which **A** is the saturation point (SP) [(T, p) at the lifting condensation level] of air near the base of the subcloud layer (at the top of the superadiabatic layer); and **D** is the SP of air from the free atmosphere sinking into the cloudy boundary layer near the mean cloud-top. The convective cloud field mixes the whole boundary layer between the surface and cloud top, but not in general, to a well-mixed structure with a single SP. In general, we would expect the vertical thermodynamic structure of the boundary layer to be characterized by a gradient of the conserved properties from near the surface to cloud top. This characteristic gradient is the mixing line (shown as a heavy dashed line) between the SPs **A** and **D**. It represents the SPs of all possible mixtures of **A**, **D**. We will use this ML as our reference process for the convective boundary layer structure and look for some vertical distribution of SP along this ML within the boundary layer, which characterizes the convective mixing process. Processes which produce deviations

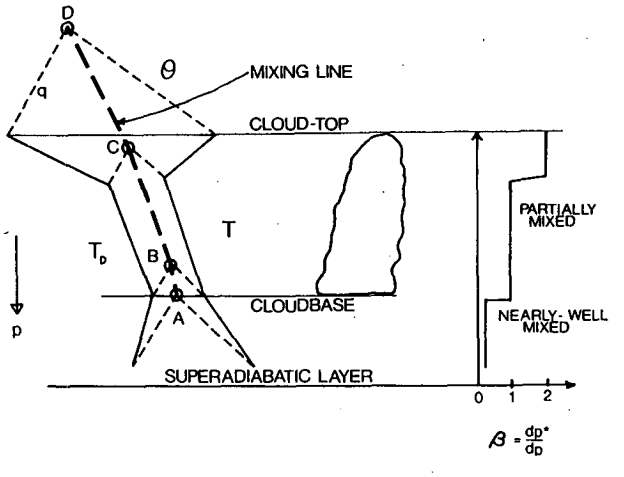

FIG. 1. Schematic tephigram of idealized cloudy boundary layer thermodynamic structure showing relationship between mixing line, temperature and dewpoint sounding in cloud and subcloud layers, and the parameter $\beta = dp^*/dp$ (see text). The dashed lines are lines of constant potential temperature and mixing ratio.

from this ML structure, such as radiative cooling in the layer, and the time dependence of the structure as a whole will be discussed in a later paper.

This idealized boundary layer is typically characterized by three regions (Ludlam, 1966; Betts, 1973). The subcloud layer is quite well mixed by the dry convective turbulence, and has only a small gradient of SP along the mixing line from **A** near the surface to **B** for the mean at cloud-base. As the subcloud layer becomes more well-mixed in θ and q, **B** approaches **A**. (For simplicity Fig. 1 does not show a cloud-base transition layer nor the superadiabatic layer near the surface.) The lower cloud layer is typically less well-mixed, with a steady trend with height of SP up the mixing line shown here as **B** to **C**. Figure 1 shows a typical shallow cumulus boundary layer where the subsaturation in this part of the cloud layer is roughly constant. Near cloud top there is a sharp change again as the transition occurs to the free atmosphere and the mixing by the cloud field falls to zero at cloud top. There is typically a stable layer in θ and a fall of q as shown, as the SP changes rapidly in the cloud-top layer to its free atmosphere value.

This vertical thermodynamic distribution can be characterized by the mixing line, and the location of an SP on it. It is convenient to use the mean saturation level $p^*(p)$ of air at a pressure level p to characterize the location of an SP on the ML. If we define a parameter β as (Betts, 1982b)

$$\beta(p) = (dp^*/dp),$$

then the thermodynamic gradients can be reconstructed from the characteristic mixing line slope (subscript M). For shallow layers these are essentially constants

$$\frac{\partial\theta}{\partial p} = \beta\left(\frac{\partial\theta^*}{\partial p^*}\right)_M ; \quad \frac{\partial q}{\partial p} = \beta\left(\frac{\partial q^*}{\partial p^*}\right)_M . \tag{1}$$

We can also define a departure from the saturation level pressure (Betts, 1982a), (related for unsaturated air to parcel subsaturation)

$$\mathcal{P}(p) = p^* - p, \tag{2}$$

so that

$$\frac{\partial\mathcal{P}}{\partial p} = \beta - 1. \tag{3}$$

We see that the three regimes in Fig. 1 have distinct values of β. The well-mixed subcloud layer has β small ($\ll 1$) so that θ, q, p^* vary only a little with height. $|\mathcal{P}|$ decreases with height in this layer with $\partial\mathcal{P}/\partial p \approx -1$ [from (3)]. The lower cloud-layer with θ, q nearly parallel to the ML, and constant subsaturation (in terms of $\mathcal{P}$), is another characteristic region of mixing with a value of $\beta \approx 1$ and $\mathcal{P} \approx$ constant; while in the cloud-top stable layer, where the convective mixing decreases to zero at cloud top, the parameter $\beta > 1$. Thus β can be regarded as characterizing the different regimes of mixing by the convection. It is a useful parameter since it can readily be determined diagnostically.

b. Characteristic profile of p(p) and β(p)*

The vertical distribution of $p^*(p)$ and $\beta(p)$ are unlikely to be the same for all convective regimes. For example, in the well-mixed stratocumulus layer (Hanson, 1984), the entire cloud and subcloud layer is thoroughly mixed to approximately a single SP, corresponding to $\beta \approx 0$ up to the cloud-top inversion. In the shallow cumulus layer by contrast, for which Fig. 1 is typical, there is some uncoupling between cloud and subcloud layers, so that the cloud layer is not as thoroughly mixed as the subcloud layer. This corresponds to a larger value of β, and indeed $\beta \approx 1$ seems typical for shallow cumulus below their cloud-top transition zone. In the transition between scattered cumulus and well-mixed stratocumulus layers, there clearly exists the possibility of intermediate values of β in the range $0 < \beta < 1$ (see section 2d). Thus, the diagnostic study of boundary layers in terms of their distribution of $p^*(p)$ provides a framework both for the classification, and an assessment of degree of mixing within and between different layers, as well as a powerful framework for a general parameterization of boundary layer structure.

Figure 2 shows an example of convective atmospheric structure over Montana in summer from a rawinsonde. A single sounding does not of course give a mean vertical structure, but it is sufficient for illustration. The heavy dashed line is the mixing line computed from the subcloud layer SP (3°C, 704 mb) and the dry air at 520 mb whose SP is at (−25.5°C, 370 mb). The open circles denote SPs within the layer from 520–700 mb: they all lie close to the dashed mixing line, indi-

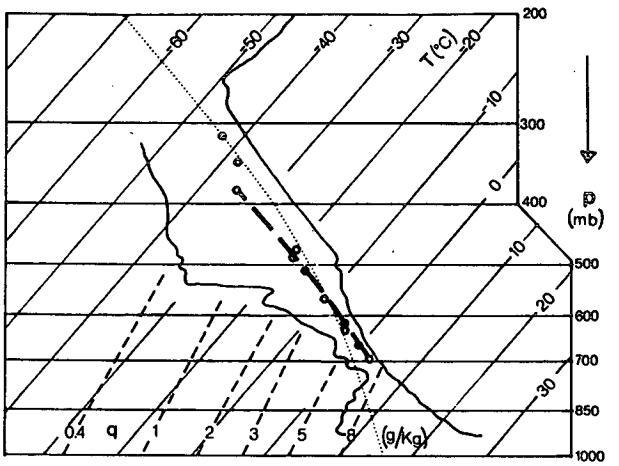

FIG. 2. Sounding at Powderville, Montana, at 1452 MDT on 6 August 1981, during the Cooperative Convective Precipitation Experiment (CCOPE) showing (T, T_D) sounding, saturation points and mixing line (heavy dashes) on a skew T–log p diagram. The dotted line is a moist adiabat.

cating that this layer is thermodynamically coupled, although it is not well-mixed. The observed weather was fair weather cumulus with some towering cumulus. The cumulus layer from 700 to 545 mb, has a mean value of $\beta \approx 1.3$. The slope $(\partial\theta^*/\partial p^*)_M$ of the mixing line is about two thirds of that of the moist adiabat.

c. Transition layers

More stable layers, with larger values of β, are characteristic of transition zones between atmospheric layers which are only partially coupled. Figure 1 does not show the cloud-base transition layer, where over a shallow layer β may exceed 1. It does show the cloud-top transition to the free atmosphere. Stable layers are associated with the overshoot cooling by convective turbulence and at cloud top by the additional cooling from liquid water evaporation (Betts, 1973; 1974; 1975).

An example of a deep transition layer capping the subcloud layer is given in Fig. 3. The sounding, again from summer in Montana, shows two overlying layers each nearly well-mixed, separated by a stable layer and sharp humidity gradient. (The upper mixed layer probably originates earlier as a boundary layer over elevated terrain.) This atmosphere as a whole has not yet been well-mixed, although at the time of the sounding a line of cumulonimbus is approaching. The mixing line (heavy dashed) shows that the subcloud layer (surface to 740 mb) and transition layer (740–675 mb) both have SPs on the same mixing line. However, they have different characteristic values of β. The subcloud layer has $\beta \approx 0.3$ and the transition layer $\beta \approx 2.5$. In this case, the slope of the mixing line is only one third of that of the moist adiabat, much more unstable than in Fig. 2. It is interesting that the subcloud layer is less well mixed with this more unstable stratification above.

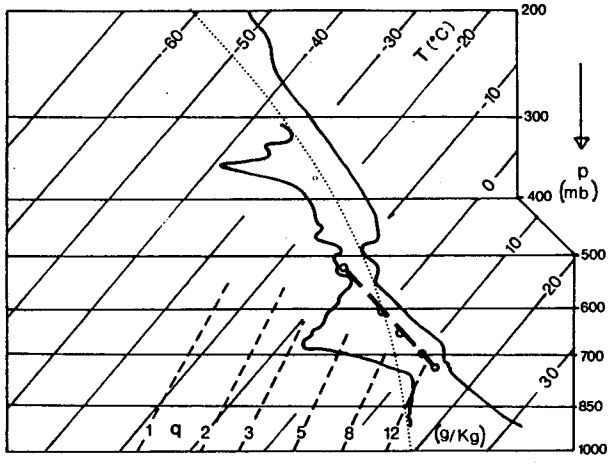

FIG. 3. As in Fig. 2 but for Miles City, Montana, at 1910 MDT 13 July 1981.

d. Mixing line slope and cloud top entrainment instability

The role of a cloud-top entrainment instability criterion as a determinant of the transition between stratocumulus and cumulus regimes has been discussed by Lilly, 1968; Randall, 1980; Deardorff, 1980; Moeng and Arakawa, 1980. Although it may not be a sufficient criterion for the breakup of a stratocumulus layer (Hanson, 1984; Randall, 1984) particularly for time-dependent boundary layers, it is an important reference. Betts (1982a) showed that this instability, which is an evaporative mixing instability, can be reduced to the comparison of the stability of the mixing line in comparison with the slope of the moist virtual adiabat (Γ_{vc}: see section 2). The cloud-scale mixing generated by this instability in cumulus will be discussed in section 4b. The instability, however, also has an important effect on the mean vertical structure in a boundary layer (the parameter β).

Consider a well-mixed but unsaturated boundary layer (driven by surface sensible and latent heat fluxes) which deepens until its top reaches the layer mean lifting condensation level and clouds form. Air from above is continually mixed into the boundary layer by turbulent entrainment, and the transition in thermodynamic properties between the subcloud layer and the air at cloud top has a mixing line structure. If this mixing line slope is more stable than the Γ_{vc} adiabat, cloud-top entrainment remains low, and the whole cloud-topped convective layer remains nearly well-mixed with $\beta \approx 0$. Further convective mixing generated by radiative cooling at cloud top helps maintain the well-mixed structure.

In contrast, if the mixing line between subcloud layer and the "free atmosphere" thermodynamics is unstable with respect to the Γ_{vc} isopleth [see (5)], the entrainment instability criterion is satisfied. Entrainment into the boundary layer is enhanced by this evaporative mixing instability, the cloud layer deepens and at the same time loses its well-mixed structure and becomes a partially cloudy cumulus layer with $\beta \approx 1$. In a sense, the cumulus layer becomes partially uncoupled from the subcloud layer because of the effect of the entrainment instability at cloud top (Deardorff, 1980).

Schematically, we might expect there to be a transition between regimes as shown in Fig. 4. However, this transition may be shifted by other factors. Strong surface fluxes will promote more thorough mixing of the convective layer and may therefore shift the curve in the sense shown, and help maintain stratocumulus despite enhanced cloud-top entrainment. This clearly needs quantitative definition and observational study. Figure 4 also shows one other schematic feature: an increase in β for the cloud layer as the mixing line approaches the slope of the Γ_{vu} isopleth (the instability criterion for unsaturated air (Betts, 1982a).

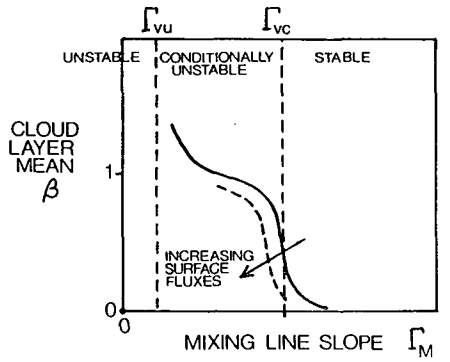

FIG. 4. Schematic showing qualitative dependence of β for the cloud layer on mixing line slope (Γ_M) across the evaporative mixing instability transition. Light dashed lines mark the dry and moist virtual adiabats (Γ_{vu} for unsaturated air and Γ_{vc} for cloudy air).

e. *Cumulus layer equilibrium*

For cumulus layers the evaporative mixing instability criterion is satisfied and cloud-top entrainment is large. We shall estimate in section 4b a velocity-scale for this turbulent mixing process: it is of order a few m s^{-1}. The cloud layer as a whole does not deepen at this rate, but instead breaks up into separate clouds and a more quiescent stably stratified environment.

The clouds continue to mix vigorously in the vertical because the mixing line is unstable for cloudy processes, and steadily deepen the convective layer by the evaporative cooling at cloud top (Betts, 1973). The layer as a whole never quite attains the mixing line structure up to cloud-top, because of this continual strong cloud-top entrainment. Figure 5 shows a θ_E, q conserved parameter plot for two soundings over Montana on 6 August 1981. The plot is similar to that introduced by Paluch (1979), although the q axis is inverted so that the plot resembles a vertical θ_E sounding. (The difference between θ_E and the wet equivalent potential temperature θ_q is small.) The soundings are close to a mixing line structure (straight line) up to the θ_E minimum (near 600 mb), where q is small. Above this level, θ_E increases with height with little change of q. Different processes are responsible for the two branches on Fig. 5. In the upper troposphere, convective mixing has been rare in this air mass, and we are seeing essentially the change of θ, θ_E at constant q associated with radiative cooling. The θ_E minimum is at the top of the convective boundary layer, and the lower atmosphere is convectively mixed down to the surface (920–930 mb) and has a corresponding mixing line structure.

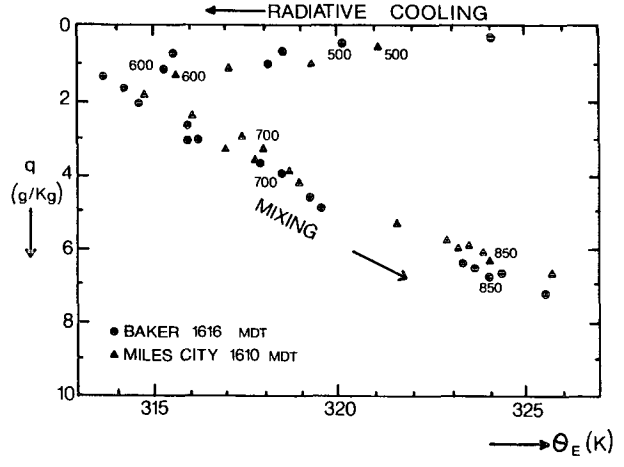

FIG. 5. Conserved parameter diagram for two soundings on 6 August 1981, during CCOPE, showing lower troposphere mixing line structure. Points are plotted for pressure levels approximately 30 mb apart: 850, 700, 600 and 500 mb p-level data are labeled approximately.

Several studies (Paluch, 1979; Boatman and Auer, 1983) have shown similar environmental profiles nearly well-mixed up to the θ_E minimum, together with in-cloud data which indicate mixing with environmental air at cloud top above the θ_E minimum. Schematically we may summarize these as in Fig. 6. Vigorous cloud towers overshoot into a layer which has not yet been modified significantly by convective mixing. With time, the environmental mixing line will move in the direction of the arrows toward the present cloud-top mixing line. However, by then, the vigorous cumulus towers will be mixing to a higher level with a corresponding new mixing line. This nonequilibrium structure with environmental SP to the left of the current cloud-top mixing line is characteristic of cumulus layers that are deepening. In convective regimes, like the tradewinds, where a steady-state cloud top is attained, large-scale subsidence and radiative cooling maintain a similar structure (Betts, 1982a). One way this can be interpreted is that both cloud and environment are adjusting toward a similar mixing line, but (in cumulus layers) the environment has a longer adjustment time (see section 4a). In stratocumulus, the large radiative divergence at cloud top can also be regarded as producing

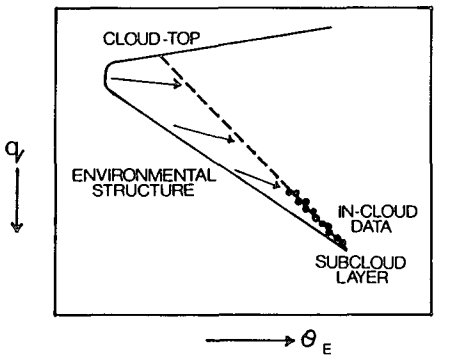

FIG. 6. Schematic showing relationship between mixing lines for cloud environment and in-cloud data, and trend of environmental structure with time (arrows).

a modified mixing line (Betts, 1983; Hanson, 1984). In this paper, however, we shall focus on the importance of the structure of $p^*(p)$ in clouds and boundary layers, rather than the processes which produce departures from one simple mixing line. The nonequilibrium structure of partially mixed convective boundary layers (an extension of the analysis of Betts, 1983) will be explored in a later paper.

For prognostic modeling of shallow cloud fields, it is sufficient to compute a cloud-top mixing line and adjust toward it with a specified adjustment time scale to approximate the convective transports in the boundary layer (see Betts and Miller, 1984).

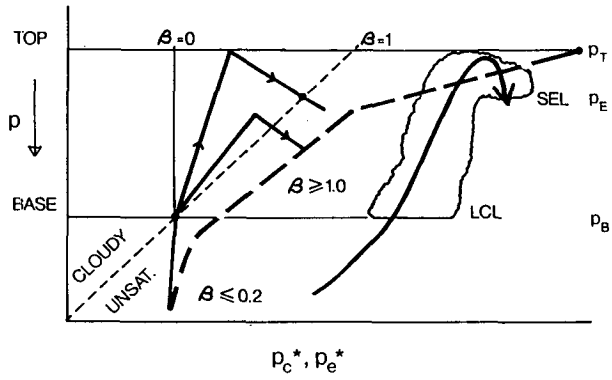

FIG. 7. Schematic tephigram showing plot of $p^*(p)$ for cloud parcels (solid lines) and environment (heavy dashed), showing separation of the two populations. A schematic air circulation through a cloud is shown on the right.

4. Cloud-scale mixing

This section discusses cloud-scale mixing in terms of the mixing line and two cloud instability processes. The first is the instability associated with cloud-top mixing and evaporation, and the second, the buoyancy equilibrium hypothesis introduced by Telford (1975), which involves the comparison of the buoyancies of cloud and environment.

a. Growing towers in scattered cumulus

A further consequence of the evaporative mixing instability is that, in boundary layers with scattered cumulus clouds, there is mixing on two separate timescales. The convective field as a whole is a vertical mixing process between the subcloud layer and the free atmosphere. The cloud environment is thermodynamically stable, while on the cloud scale there is vigorous vertical mixing because the cloudy regions are unstable to cloudy processes. This affects both the bulk thermodynamics of the cloud (e.g., Paluch, 1979) and also the microphysics (e.g., Baker and Latham, 1979). These are complex processes which perhaps may not be easily reduced to simple parameters. However, for simple cloud parameterizations and the representation of subgrid scale cloud statistics in numerical models, a bulk representation of cloud-scale mixing would have value.

For the simplified quasi-equilibrium structure discussed in section 3, where the cloud layer is characterized by a unique mixing line, in-cloud thermodynamic properties will also have SPs on this mixing line, and could be characterized by a saturation level (SL) distribution $p_c^*(p)$ for cloudy air. Figure 7 shows a possible model in the form of a schematic plot of p^* against p, showing how the distinct cloud–environment populations might stratify in a diagnostic study. The short dashed line is $p = p^*$, representing the boundary between cloud and unsaturated air, between unstable and stable regions. The levels where cloud-parcels cross this boundary are significant in the atmosphere. They are cloud base or lifting condensation level (LCL), and the level at which overshooting cloud tops sink and evaporate completely (called the sinking evaporation level, SEL, in Betts, 1978). The heavy dashed line is the environmental mean profile showing the typical structure discussed in Fig. 1, with p^* varying slowly with p in the subcloud layer (small $\beta \approx 0.2$), a cumulus layer with nearly constant subsaturation ($\beta \approx 1$), and a cloud-top stable layer where p^* increases to its free atmosphere value at cloud top, p_T. Although the thermodynamic structure is characterized by one mixing line there are quite distinct zones of mixing and a very nonuniform $p^*(p)$ distribution (as in Fig. 1).

Schematic paths of $p_c^*(p)$ (corresponding to different values of β_c) are drawn for two cloud parcels rising with mixing from cloud base, overshooting to reach cloud top at p_T and sinking back to become part of the environment near the base of the cloud-top stable layer. Mixing between cloud and environment gives nonadiabatic thermodynamic parameters inside the cloud and corresponds to $\beta_c > 0$. A wide range of mixing is likely to exist, but it is possible that the cloud towers of the deeper clouds may have a characteristic value of β_c. The deeper clouds are an important subset of the population because they determine the depth of the convective layer. In addition they will be the first to form precipitation-size particles. Observations of cloud top and the SEL (the level where sinking cloud towers evaporation) for these clouds could be used to estimate mean values of β_c over the ascent and descent of a parcel through the cloud. Betts (1982b) showed that

$$\frac{p_E - p_T}{p_B - p_T} = \frac{1 - \beta_c}{1 + \beta_c} \tag{4}$$

where p_B, p_T, p_E are the pressure levels for cloud base, cloud top and the SEL (Fig. 7) respectively. Thus for $\beta_c = 0.5$, clouds sink back one-third of the distance to cloud base before evaporating. These estimates of β_c

could be compared with bulk estimates of mixing from in-cloud thermodynamic measurements.

The estimation of the *level of origin* of air entrained into clouds from their environment (Paluch, 1979; Boatman and Auer, 1983; LaMontagne and Telford, 1983) requires an environmental structure which departs from this one mixing line, hypothesized for a quasi-equilibrium balance between subsidence and convection. In fact, cumulus layers rarely attain the hypothesized equilibrium mixing line structure throughout their entire depth, because nonprecipitating convection is inherently destabilizing (Betts, 1973) and the cloud field continually deepens, entraining unmodified air at cloud top as discussed in (3e) and Fig. 6. Despite this, the single parameter $p^*(p)$ representation gives a good estimate of the relative fractions of air *originating* from below cloud-base and at the top of the convective layer, and is an important diagnostic parameter as a tracer on air parcel saturation level.

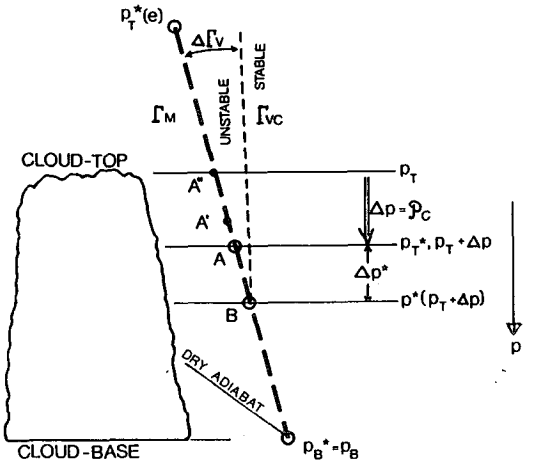

FIG. 8. Schematic tephigram showing mixing line (heavy dashes) for evaporative mixing instability: $p_T^*(e)$ is the saturation level (SL) of environmental air entrained at cloud-top (pressure level p_T); p_T^* is the SL of cloudy air below the cloud-top interface.

b. *Energetics of evaporative mixing instability*

Many authors have discussed the importance of cloud-top evaporative mixing instability: Lilly (1968), Randall (1980), Deardorff (1980) for stratocumulus; Squires (1958), Paluch (1979) and others for cumulus. Betts (1982a) showed it is related to the mixing line slope being more unstable than the moist virtual adiabat (Γ_{vc}, section 2). It is a within-cloud instability and as pointed out by Randall (1980) it is essentially the classical conditional instability, with virtual temperature included. It is a mixing instability as well because the turbulent overturning mixes in unsaturated air at cloud top, which in turn maintains the unstable mixing line slope. Without this entrainment, the cloud layer would overturn and establish a neutral structure (SPs on Γ_{vc} isopleth). However, moist adiabatic descent is limited by the parcel liquid water content (Betts, 1973), which can be further reduced by mixing. Note that is an instability within the cloud, and is distinct from the comparison of cloud–environment buoyancy differences, which is discussed in section 4c.

We shall use the simple mixing line model to illustrate the energetics of this process, and establish a time scale and turbulent velocity scale for the instability, which should be of importance to cloud-top entrainment instability, and downward mixing from cloud top in cumulus.

Figure 8 shows a schematic thermodynamic diagram where cloud-top mixing has established a gradient of SL, p^* *within* the cloud along a mixing line as shown. The slopes of the mixing line and the moist virtual adiabat will be linearized and defined symbolically in terms of the gradient of virtual potential temperature for unsaturated air, θ_{vu}, (see Betts, 1982a).

$$\Gamma_M = (\partial\theta_{vu}/\partial p)_M; \quad \Gamma_{vc} = (\partial\theta_{vu}/\partial p)_{\theta_{vc}};$$
$$\Delta\Gamma_v = \Gamma_{vc} - \Gamma_M$$

is a measure of the instability of the mixing line for cloudy processes.

Consider a cloud parcel just below cloud top, p_T, with SL, p_T at A. Its liquid water content is related to $\mathcal{P}_c = p_T^* - p_T$. Any small downward perturbation will produce unstable descent, but without further mixing it will evaporate all its liquid water (l) after descending a pressure distance $\Delta p = \mathcal{P}_c$ to its SL, p_T^*. If the bulk of the cloud at this new *pressure* level ($p_T + \Delta p$) has a SL $p^*(p_T + \Delta p)$ as shown (point **B**) then the perturbed parcel will have a negative buoyancy (as its liquid water reaches zero) of

$$\Delta\theta_v = \Delta\Gamma_v \Delta p^*. \tag{5}$$

Hence, we can define an evaporative available potential energy (EAPE) for this descent while cloudy

$$\text{EAPE} = g\,\frac{\overline{\Delta\theta_v}}{\theta_v}\,\Delta z. \tag{6}$$

Using (5) and converting to pressure units, using mean panel density ρ

$$\text{EAPE} = \frac{g\Delta\Gamma_v}{2\theta_v}\,\Delta p^*\,\frac{\Delta p}{\rho g}. \tag{7}$$

Now $\Delta p = \mathcal{P}_c$ and $\Delta p^* = \beta\Delta p$, if we use the parameterization from section 3, giving

$$\text{EAPE} = \frac{\beta}{2(\rho g)^2}\left(\frac{\mathcal{P}_c}{\tau}\right)^2, \tag{8}$$

where an evaporative mixing instability time scale has been defined

$$\tau = \left(\frac{\rho g^2 \Delta\Gamma_v}{\theta_v}\right)^{-1/2}. \tag{9}$$

As well as this instability time scale, it is clear that there is an associated velocity scale (in p-coordinates)

$$\Omega_E = a\mathcal{P}_c/\tau, \quad \text{where} \quad a = \sqrt{\beta/2} \approx 0.5, \quad (10)$$

related to the descent distance before total evaporation of cloud water. In cumulus we might expect $\Delta\Gamma_v \approx 2°C/100$ mb and $\mathcal{P}_c \approx 50$ mb (equivalent to $l \approx 1.0$ g kg^{-1}) we find $\tau \approx 120$ s, $\Omega_E/\rho g \approx 2$ m s^{-1}.

For cloud-top entrainment instability in stratocumulus, the time scale will be longer near the marginal instability condition, and l may be less. For $\Delta\Gamma_v \approx 0.5°C/100$ mb and $\mathcal{P}_c \approx 10$ mb we find a smaller $\Omega_E/\rho g \approx 20$ cm^{-1}. We would expect Ω_E to be a useful scaling parameter for turbulent entrainment.

This simple analysis neglects three factors. As $\beta \rightarrow 0$ (a well-mixed layer) EAPE appears to vanish in (8). However, whatever the gradient of $p^*(p)$ within the cloud layer, there will always be a gradient at the cloud-top interface. One can modify the analysis and consider an initial "perburbation" to be caused by additional mixing moving A to A′ on the ML. This parcel is colder at cloud top (p_T) but it also has a smaller $\mathcal{P}_c$ and l, so that its cloudy descent distance is reduced. It is straightforward to find a maximum EAPE for various A′ between A and A″. The appendix shows that only the coefficient in (8) is changed:

$$(\text{EAPE})_{\max} = \frac{1}{2(\rho g)^2(2-\beta)}\left(\frac{\mathcal{P}_c}{\tau}\right)^2. \quad (8')$$

This reduces to (8) for $\beta = 1$, but is non-zero for $\beta = 0$. Secondly, a parcel is negatively buoyant after descent to zero liquid water content, and will then descend dry adiabatically conserving its (unsaturated) θ_{vu} (in the absence of further mixing). This increases the coefficient on EAPE in (8) (see appendix) but the effect is small, provided the mixing line slope is closer to the Γ_{vc} than the Γ_{vu} isopleth. The third simplification is that in estimating Ω_E, it was assumed that there was no further mixing after a parcel started its unstable descent. This focuses attention on a difference between updrafts and downdrafts in nonprecipitating cumulus. Mixing sets up the unstable mixing line structure within clouds. Parcels perturbed downwards can sink in a downdraft until they evaporate all their cloud water, whereas parcels perturbed upwards have no such restriction. Continual mixing reduces the buoyancy perturbation for both updrafts and downdrafts, but for downdrafts it also permits unstable descent to continue by supplying more cloud water. Emanuel (1981) has proposed a similarity theory for unsaturated downdrafts in cumulus, based on continuous mixing and evaporation. Despite these complications, it still seems likely that the velocity scale ($\mathcal{P}_c/\tau$) may be an important scaling parameter for evaporative mixing instability.

c. *Telford's buoyancy equilibrium hypothesis*

Telford (1975), Telford and Wagner (1980) and Rogers *et al.* (1985) have proposed that the cumulus lifecycle has three distinct phases. Newly growing towers form on the upshear side of clouds, then mix rapidly to near buoyancy equilibrium with the cloud environment. They suggest that the bulk of the cloud lasts for a relatively long time in this "dwell-phase," mixing more slowly until, once it becomes negatively buoyant, it sinks as a whole and rapidly evaporates. This argument involves a comparison of the buoyancy of cloud and environment at the same level, in contrast to section 4b where the vertical instability within the cloud alone was analyzed ignoring the environmental stratification. By using a mixing line analysis we can explore the relationship of these two overturning processes on different scales.

1) BUOYANCY EQUILIBRIUM AND LIQUID WATER CONTENT

The idea of a reference liquid water content associated with neutral buoyancy (Telford and Wagner, 1980) is of value because on a single mixing line, buoyancy and liquid water content have a one-to-one relationship at any pressure level in a cloud. We again linearize the slope of this mixing line and the reference θ_v isopleths for unsaturated and cloudy air, Γ_{vu}, Γ_{vc} (Betts, 1982a), using the definitions of Γ_M and Γ_{vc} in section 4b, and noting $\Gamma_{vu} = (\partial\theta_{vu}/\partial p)_{\theta_{vu}} = 0$. Figure 9 shows a schematic thermodynamic diagram. By equating the change of θ_{vu} along the heavy dashed mixing line to the change along the dashed virtual adiabats which intersect at Q, we get the buoyancy equilibrium condition:

$$\Gamma_M(\mathcal{P}_{cn} - \mathcal{P}_c) = \Gamma_{vc}\mathcal{P}_{cn} \quad (11)$$

where $\mathcal{P}_c$, $\mathcal{P}_e$ are $(p^* - p)$ for cloud and environment at any level and suffix n denotes neutral buoyancy. This gives a condition on l_n and $\mathcal{P}_{cn}$

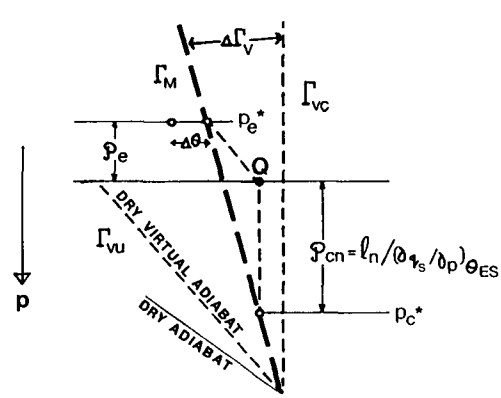

FIG. 9. Schematic thermodynamic diagram showing relationship of mixing line, $\mathcal{P}$, and cloud liquid water content to buoyancy equilibrium hypothesis. The open circles denote environment and cloud parcel SPs.

$$l_n/(\partial q_s/\partial p)_{\theta ES} = \mathcal{P}_{cn} = \mathcal{P}_e\Gamma_M/(\Gamma_M - \Gamma_{vc}), \quad (12)$$

which involves the environmental subsaturation $\mathcal{P}_e$ and the mixing line slope in relation to the reference density isopleths. Typically for cumulus layers, Γ_M may lie halfway between Γ_{vu}, Γ_{vc}; $\mathcal{P}_e \approx 50$ mb (usually varying only weakly with height: $\beta_e \approx 1$: see section 2), giving for neutral buoyancy

$$\mathcal{P}_{cn} \approx 50 \text{ mb}, \quad l_n \approx 1.0 \text{ g kg}^{-1} \quad (13)$$

roughly independent of height in the cloud. This simple formulation breaks down near cloud base where even adiabatic cloud parcels are typically negatively buoyant and the environmental SPs lie off the cloud-top mixing line (for example, see Betts, 1982a, Fig. 16). However, it is qualitatively a reasonable approximation for the upper half of a cloud layer. Environmental SPs off the cloud-top mixing line ($\Delta\theta$ at constant p in Fig. 9), can be included to give a modified formula

$$\mathcal{P}_{cn} = \frac{\mathcal{P}_e\Gamma_M - \Delta\theta}{(\Gamma_M - \Gamma_{vc})}, \quad (12')$$

showing that an environmental SP structure to the left of the cloud-top mixing line reduces the neutral buoyancy liquid water content.

2) DWELL PHASE EQUILIBRIUM

Having defined $\mathcal{P}_{cn}(p)$ using (12'), we can say that a region of a cloud is buoyant compared to its environment if $\mathcal{P}_c > \mathcal{P}_{cn}$ and is therefore likely to maintain a cloud-base updraft, but if $\mathcal{P}_c < \mathcal{P}_{cn}$ it is negatively buoyant, and is likely to sink and rapidly evaporate. Clearly $\mathcal{P}_{cn}$ gives a valuable point of reference for the future of a cloud.

However, if the evaporative mixing instability criterion is met ($\Delta\Gamma_v > 0$ in Fig. 8) then downward mixing from cloud top will proceed continuously because of the mechanism discussed in section 4b, regardless of $\mathcal{P}_c$, and $\mathcal{P}_c$ will decline steadily at all levels as mixing proceeds. It seems unlikely therefore that a long-lasting dwell phase can exist at neutral buoyancy. Vertical advection (that is an updraft) is needed to balance the continuous downward mixing in order to attain any quasi-steady state, and this requires a slightly buoyant cloud with $\mathcal{P}_c > \mathcal{P}_{cn}$.

We can set up a simple one-dimensional model to describe this. Neglecting horizontal gradients, we would write the SL balance at a pressure level as

$$\frac{\partial p_c^*}{\partial t} + \omega_c\frac{\partial p_c^*}{\partial p} = \omega_{\text{mix}} \quad (13)$$

where p_c^*, ω_c are respectively mean SL and vertical velocity (in p-coordinates) in the cloud at a pressure level. Cloud parcel SL is not conserved following a parcel because of downward mixing of air with a SL at a lower pressure, which we parameterize as a velocity scale, ω_{mix}. For the maintenance of the cloud with time, we require

$$\partial p_c^*/\partial t > 0 \quad \text{or} \quad \beta = \partial p_c^*/\partial p < \omega_{\text{mix}}/\omega_c.$$

We see that (for constant ω_{mix}) stronger updrafts will give smaller values of β_c corresponding more closely to adiabatic ascent. For the maintenance of the cloud with height we require $\partial p_c^*/\partial p < 1$ which means $|\omega_c| > |\omega_{\text{mix}}|$. In cumulus, ω_{mix} is probably $<\Omega_E \approx$ few m s^{-1}, although it is likely to be related to the updraft energetics as well. This suggests that the maintenance of a cloud requires a certain updraft sufficient to balance the downward mixing of air with a lower SL pressure. If the updraft weakens below this value, the cloud will rapidly die. We conclude that a "dwell phase" (Telford and Wagner, 1970) of a cloud is possible, but that it requires weak positive buoyancy rather than buoyancy equilibrium. Although we have concluded a dwell phase is possible, we have not explained why it might occur.

The maintenance of a 3 m s^{-1} updraft in a 1.5 km deep cloud requires only weak positive buoyancy, ($\approx$0.2 K) corresponding to small values of $(\mathcal{P}_c - \mathcal{P}_{cn}) \approx 10$ mb for $\Gamma_M \approx 2°/100$ mb, appreciably smaller than our estimate of $\mathcal{P}_{cn} \approx 50$ mb. Thus, it seems that the idea of buoyancy equilibrium and corresponding values of l_n, $\mathcal{P}_{cn}$ is a useful reference point.

d. Updraft energetics

An estimate of the *cloud-scale* updraft available potential energy (UAPE) can be made using buoyancy equilibrium as a reference state [Eq. (12)]. Using mean values for a cloud of depth Δp

$$\text{UAPE} \approx g\frac{\overline{\Delta\theta_v}}{\theta_v}\frac{\Delta p}{\rho g}. \quad (14)$$

Using an analysis similar to that in section 4c and Fig. 9 one can introduce a mean $\bar{\mathcal{P}}_{cn}$ (Eq. 12) giving

$$\text{UAPE} \approx g\Delta\Gamma_v(\bar{\mathcal{P}}_c - \bar{\mathcal{P}}_{cn})\Delta p/\rho g\theta_v, \quad (15)$$

which gives an estimate of an updraft Ω_u [defining τ from (9)]

$$\Omega_U \approx (\Delta p(\bar{\mathcal{P}}_c - \bar{\mathcal{P}}_{cn})/\tau)^{1/2}. \quad (16)$$

Equation (16) shows that cloud depth is an important scaling parameter for the cloud-scale updraft velocity as well as $\mathcal{P}_c$ (related to cloud water) and $\mathcal{P}_{cn}$ (related to the environmental and mixing line stratification). Equation (16) has a well-known and important upper limit. In the absence of mixing, cloud water will have the adiabatic values and $\bar{\mathcal{P}}_c \approx \Delta p/2$, and for some cumulus atmospheres $\bar{\mathcal{P}}_{cn}$ is small, giving

$$\Omega_U(\text{max}) < \Delta p/\tau. \quad (17)$$

e. Distribution of p^* within clouds

Sections 4c and 4d discuss highly simplified models of the updraft and downdraft energetics which show that $\mathcal{P}_c$ is an important pressure scale in addition to layer depth Δp and $\mathcal{P}_{cn}$, which is related to environmental structure and mixing line slope. Clouds are very inhomogeneous however, and we need observational studies of the distribution of p^* (and hence $\mathcal{P} = p^* - p$) to assess the usefulness of these parameters for the study of mixing within clouds. Nonetheless, because the vertical mean structure is tied to a mixing line (or closely related structure), the statistics of the p^* distribution do reflect both the vertical transports and the horizontal mixing between updraft and downdrafts and may yield information about the complex circulation within clouds. Furthermore, because Eq. (13) suggests that the p^* structure within clouds may represent primarily a balance between downward mixing by evaporative mixing instability and upward advection by the mean cloud-scale circulation, it is possible that it may be useful to look for functional relationships of the form

$$\beta = f(\Omega_E/\Omega_U). \tag{18}$$

For partly cloudy boundary layers the distribution of p^* within clouds is just part of the whole p^* distribution of cloud and environment, discussed in the next section.

5. Statistical structure in cloudy boundary layers

Section 3 discussed parametric models for the mean vertical structure of partially cloudy boundary layers, and section 4 some aspects of the thermodynamic structure and processes within clouds. The cloud–environment separation is a conceptual idealization, similar to the ascending–descending branch separation in a mixed stratocumulus layer (Betts, 1983). Both though, are interrelated with the fractional cloud cover which is important to the radiative budgets of the earth's boundary layer. In the final section of this paper, we shall discuss in outline only the structure of p^* within a boundary layer from a statistical viewpoint.

a. Data sampling

Following earlier sections, we assume that the thermodynamic structure is characterized by one mixing line, so that the saturation level, p^*, on this ML uniquely defines a parcel's thermodynamic properties, whether cloud or environment. In the primary section we have discussed only the mean vertical distribution of $p_c^*(p)$, $p_e^*(p)$ for cloud and environment. *In-situ* vertical sampling whether by aircraft or balloon soundings gives instantaneous profiles rather than the mean structure. Horizontal sampling gives the statistics of the distributions of $p^*(x, y)$; a measure of the variance at each level. If the horizontal distribution is combined with a vertical mean profile, then it can be converted to a distribution of air parcels, originating in the mean at different levels in the atmosphere, which have ascended or descended with the vertical motions in clouds and between clouds. (Parcels with $p^* > p$ are cloudy, while those with $p^* < p$ are unsaturated.) Clearly, the horizontal distribution $p^*(x, y)$ [together with the vertical mean structure of $p_c^*(p)$ and $p_e^*(p)$] encapsulate the statistics of the boundary layer mixing process and the fractional cloud cover. Observational studies are needed to provide these statistics and their height variation for different cloud regimes. For illustration, a normal distribution will be considered first.

b. Normal distribution

A normal distribution of p^* at a pressure level would give a particularly simple relationship between mean p^*, distribution variance and fractional cloudiness. Figure 10 shows this schematically for a level mean subsaturation pressure $\bar{\mathcal{P}} = (p^* - p)$, and a normal distribution with a variance $\sigma = |\bar{\mathcal{P}}|$ (chosen only for illustrative simplicity). The bulk of the distribution corresponds to unsaturated air (with $p^* < p$), only the tail greater than $+\sigma$ corresponds to cloudy air. Hence, for this case, the fractional cloudiness is $\approx 16\%$ (see cumulative distribution on right).

We see that given the distribution $N(p^*, p)$ (a function of pressure), fractional cloudiness is specified. Very simple parameterizations may be of value in models. For example, if the mean $\bar{\mathcal{P}}$ is given by $\partial\bar{\mathcal{P}}/\partial p = \beta - 1$, integrated from cloud base, and the distribution is normal, we need only σ to give cloudiness as a function of height. For the very simple case of σ independent of height, the fractional cloudiness changes with height only through the shift of the mean of the distribution as $\bar{\mathcal{P}}$ changes.

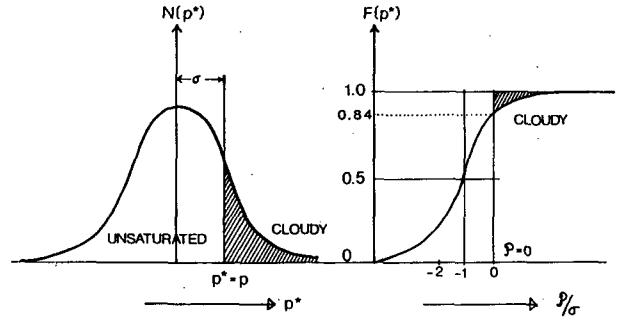

FIG. 10. Schematic showing distribution function $N(p^*)$ at a pressure level p. Distribution is normal with mean p^* offset $\bar{\mathcal{P}}$ (negative) from p corresponding to the mean subsaturation at that level and standard deviation σ. On the right is the cumulative distribution function expressed in multiples of $\mathcal{P}/\sigma$, showing fractional cloudiness ($\mathcal{P} > 0$) $\approx 16\%$.

c. *Other distributions*

It would be surprising if a normal distribution fitted most real boundary layers. Diagnostic studies which are particularly simple in the (p, p^*) framework, or the computation of distributions from the numerical simulation of cloud fields, are needed as a basis for further parameterizations. However, we will discuss some possible complications. The conventional model distinctions of cloud and environment (or ascending and descending branches) imply bimodal distributions of $N(p^*)$, not normal distributions. Indeed for the model mixed stratocumulus layer in Betts (1983, Fig. 1), the idealized distribution has two very sharp peaks for the ascending and descending branches of the symmetric circulation, so that fractional cloudiness changes discontinuously from 100 to 50% as p passes p_D and to 0% as p passes p_A (p_D, p_A are the cloudbases for the descending and ascending branches, respectively).

For a cumulus field discussed in earlier subsections the concept of different values of β for cloud and environment implies distinct peaks whose separation changes with pressure. Figure 11, arranged with p^* vertical, shows hypothetical distributions at different levels in the boundary layer. Near the surface a near normal distribution $N(p^*)$ with a peak at or a little below cloud-base (here assumed to be 900 mb) may be a reasonable approximation. However, in the cloud layer, if there are characteristic peaks for cloudy and environmental air corresponding to $\beta_c = 0.5$ and $\beta_e = 1.0$, then a bimodal distribution function with separating peaks is likely as shown schematically.

One reason to expect a bimodal distribution for a cumulus layer is that air with $p^* = p$ ($\mathcal{P} = 0$) has the minimum temperature associated with cloud–clear air mixing at a cloud boundary (Betts, 1982a). This air at the evaporating cloud boundary will have a maximum negative buoyancy for that level, and might be expected to sink rapidly to nearer its level of buoyancy equilibrium. The concept of buoyancy equilibrium (Telford, 1975; Telford and Wagner, 1980) would also suggest a bimodal distribution with peaks for cloud and environment at values of $\mathcal{P}_{cn}$, $\mathcal{P}_e$ satisfying Eq. (12). However, clouds may have a broader p^* distribution with some active towers having, say, $\beta_c \approx 0.5$, while a larger cloud residue has weak updrafts and is slowly decaying near buoyancy equilibrium (with perhaps $\beta_c \approx 0.8$). This is an important difference. Most in-cloud measurements focus on the properties of active clouds. However, for the computation in models of the radiative fluxes in the boundary layer we require the entire cloud distribution.

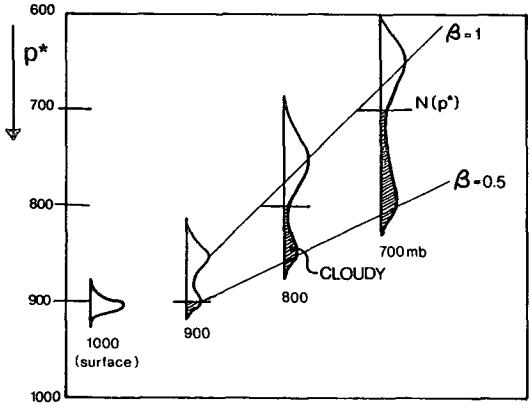

FIG. 11. Schematic showing hypothetical $N(p^*)$ distributions for four pressure levels, surface (1000 mb), cloud-base (900 mb), 800 mb and 700 mb. Peaks assume distinct separation of cloud and environment populations, with different characteristic values of β.

These examples are only schematic. The intent is to suggest a general framework for the analysis of cloud field thermodynamic data using a mixing line approach and particularly (p^*, p) coordinates, which is suitable for the diagnostic analysis of cloud fraction in terms of a measurable thermodynamic distribution. They also form a framework for the study of vertical mixing (e.g., change of mean with height) and horizontal mixing between cloud and environment or ascending and descending branches in boundary layers (related to variance of p^* at a level and separation of distribution peaks). The spectrum could also form the basis for the study of the final decay and evaporation of clouds by mixing processes.

6. Conclusions

This paper has presented a diagnostic framework for the study of partially mixed cloudy boundary layers, in-cloud properties and fractional cloudiness using bulk thermodynamic methods. We have shown how choosing a representative mixing line between the subcloud layer and air entrained at cloud top can be used to simplify the boundary layer mixing problem into the study of air parcel saturation level, p^*, which locates a parcel's thermodynamics on the mixing line. The mean distribution of $p^*(p)$ for cloud and environment are important bulk properties of a layer.

If the air at cloud top is stable to evaporate mixing instability then the boundary layer becomes quite well-mixed with a small internal gradient of $p^*(p)$. However, if cloud-top entrainment satisfies the evaporative mixing instability criterion, then cloud-top mixing becomes a rapid downward mixing process and the layer as a whole becomes partially cloudy with a mean gradient $\partial p^*/\partial p \approx 1$. Thus, the rapid cloud-top entrainment partially decouples the cloud layer from the subcloud layer to give the layered thermodynamic structure of scattered cumulus. The transition between stratocumulus and cumulus can be studied using the mixing line, and this $p^*(p)$ framework.

A velocity scale for the evaporative entrainment instability is derived. For cumulus it is ~few m s^{-1}; near the stratocumulus breakup condition it may be an order of magnitude less. We discuss the buoyancy equilibrium condition proposed by Telford for liquid water content in cumulus, and conclude that a quasi-steady state requires weak positive buoyancy so that upward advection can balance downward mixing by the evaporative mixing instability. A velocity scale for cloud-scale updrafts was estimated in terms of a departure from this buoyancy equilibrium condition.

The distribution function along a mixing line of air parcel p^* at one pressure level is related to fractional cloudiness. A normal distribution gives a particularly simple relationship between the cumulative frequency distribution and fractional cloudiness. Diagnostic studies are needed of actual distributions in partially cloudy boundary layers of all types (as a function of height) to provide an observational basis for parametric models of fractional cloudiness. It is likely that a bimodal distribution exists for many cumulus layers.

The major limitation of this paper is that it provides only a conceptual framework. Extensive data analysis of a wide range of boundary layers are needed to provide the statistical structure of different boundary layers and cloud fields, in terms of the conserved parameter mixing line. The few published examples (Betts, 1982, 1984; Hanson, 1984; Paluch, 1979; Boatman and Auer, 1983; LaMontagne and Telford, 1983) for boundary layer structure give encouragement that this analysis approach will be fruitful. Global modeling work is in progress (Betts and Miller, 1984) using a mixing line parameterization for shallow convection based on these preliminary diagnostic studies, also with encouraging results. There is no doubt that proper inclusion of the vertical thermodynamic transports by shallow nonprecipitating (or weakly precipitating) cloud fields is crucial for global modeling. It is hoped that diagnostic analyses of the type proposed here will provide an observational basis for the improvement of current schemes. In addition, observational studies will provide the basis for the inclusion of radiative and other nonequilibrium processes, which produce deviations from the idealized mixing line structure considered in this paper.

Acknowledgments. This work has been supported by the Global Atmospheric Research Program of the Atmospheric Sciences Section of the National Science Foundation under grant ATM-8403333, and the National Aeronautics and Space Administration, Goddard Space Flight Center, under contract NAS5-28590.

APPENDIX

Downdraft Available Potential Energy from Evaporative Mixing

In section 3b, the evaporative available potential energy (EAPE) for parcel descent with evaporation was computed for SP A in Fig. 8, which becomes negatively buoyant on descent. The expression (8) vanishes though, within a well-mixed layer with $\beta = 0$. However, at cloud top, mixing will still produce negative buoyancy.

a. Maximum EAPE from mixing

We can initiate unstable parcel descent by mixing. Conceptually we suppose the same mean gradient $\beta = \partial p^*/\partial p$ within the cloud. Rather than perturb parcel A (in Fig. 5) downward, suppose there is locally additional downward vertical mixing, changing its SP to A′ (here we show this at cloud top), where A′ is cloudy with $(p^* - p)$ of $\alpha\mathcal{P}_c (0 < \alpha < 1)$. As α changes from 0 to 1 this corresponds to all mixtures from A″ to A on the mixing line, and liquid water contents from zero to that corresponding to $\mathcal{P}_c$. The parcel with SP at A′ has less liquid water but greater initial negative buoyancy. Its initial buoyancy is

$$\Delta\theta_v(I) = \Delta\Gamma_v(1 - \alpha)\mathcal{P}_c, \tag{A1}$$

its final value, as $l \to 0$ after descending $\alpha\mathcal{P}_c$ in cloud with $\partial p^*/\partial p = \beta$,

$$\Delta\theta_v(F) = \Delta\Gamma_v[(1 - \alpha)\mathcal{P}_c + \beta\alpha\mathcal{P}_c]. \tag{A2}$$

Hence its integrated

$$\text{EAPE} = \frac{g\Delta\Gamma_v}{2\theta_v}[2(1 - \alpha) + \beta\alpha]\alpha\frac{\mathcal{P}_c^2}{\rho g}. \tag{A3}$$

For $\alpha = 1$, this reduces to (8). Differentiating gives a maximum value of EAPE for $\alpha = 1/(2 - \beta)$ of [using (9)]

$$(\text{EAPE})_{\max} = \frac{1}{2(\rho g)^2(2 - \beta)}\frac{\mathcal{P}_c^2}{\tau^2} = \left(\frac{\Omega_E}{\rho g}\right)^2 \Big/ (4 - 2\beta). \tag{8′}$$

For $\beta = 1$, this is the same as (8), but for $\beta = 0$, EAPE is not zero but is reduced only by a factor of 2.

b. Subsequent unsaturated descent

A further extension is to consider the additional contribution to the downdraft available potential energy from the unsaturated descent of a parcel after all cloud water is evaporated (if there is no further mixing). Its negative buoyancy will decrease from that given by (A2) to zero (buoyancy equilibrium) after sinking:

$$\Delta p = \Delta\theta_v(F)/(\partial\theta_v/\partial p)_c, \tag{A4}$$

where the gradient of θ_v in the cloud layer is given by

$$\left(\frac{\partial\theta_v}{\partial p}\right)_c = \beta\left(\frac{\partial\theta_{vu}}{\partial p^*}\right)_M + (1 - \beta)\left(\frac{\partial\theta_{vu}}{\partial p^*}\right)_{\theta_{vc}} = \Gamma_{vc} - \beta\Delta\Gamma_v \tag{A5}$$

where $\Gamma_{vc} = (\partial\theta_{vu}/\partial p)_{\theta_{vc}}$. This is a weighted average between the gradients for the mixing line and the θ_{vc} isopleth. The additional APE contribution for this unsaturated descent is therefore

$$\text{EAPE}' = \frac{[(1-\alpha)+\alpha\beta]^2}{2(\rho g)^2}\frac{\mathcal{P}_c^2}{\tau^2}\frac{\Delta\Gamma_v}{\Gamma_{vc}-\beta\Delta\Gamma_v}. \quad \text{(A6)}$$

This contribution is small compared to EAPE for mixing line slopes close to the Γ_{vc} isopleth (small $\Delta\Gamma_v/\Gamma_{vc}$) but may become significant for very unstable mixing lines. However, we see that it retains the same proportionality to Ω_E^2 as (8) and (8′).

REFERENCES

Arakawa, A., and W. Schubert, 1974: Interaction of a cumulus cloud ensemble with the large-scale environment: Part I. *J. Atmos. Sci.*, **31**, 674–701.

Baker, M. B., and J. Latham, 1979: The evolution of droplet spectra and the rate of production of embryonic raindrops in small cumulus clouds. *J. Atmos. Sci.*, **36**, 1612–1615.

Betts, A. K., 1973: Non-precipitating cumulus convection and its parameterization. *Quart. J. Roy. Meteor. Soc.*, **99**, 178–196.

——, 1974: Reply to (Comments on non-precipitating cumulus convection and its parameterization). *Quart. J. Roy. Meteor. Soc.*, **100**, 469–471.

——, 1975: Parametric interpretation of trade-wind cumulus budget studies. *J. Atmos. Sci.*, **32**, 1934–1945.

——, 1978: Convection in the tropics. *Meteorology over the Tropical Oceans.* Quart. J. Roy. Meteor. Soc., D. B. Shaw, Ed., 105–132.

——, 1982a: Saturation point analysis of moist convective overturning. *J. Atmos. Sci.*, **39**, 1484–1505.

——, 1982b: Cloud thermodynamic models in saturation point coordinates. *J. Atmos. Sci.*, **39**, 2182–2191.

——, 1983: Thermodynamics of mixed stratocumulus layers: Saturation point budgets. *J. Atmos. Sci.*, **40**, 2655–2670.

——, 1984: Boundary layer thermodynamics of a high plains severe storm. *Mon. Wea. Rev.*, **112**, 2199–2211.

——, and M. J. Miller, 1984: A new convective adjustment scheme, ECMWF Tech. Rep. No. 43, ECMWF, 68 pp.

Boatman, J. F., and A. H. Auer, 1983: The role of cloud top entrainment in cumulus clouds. *J. Atmos. Sci.*, **40**, 1517–1534.

Deardorff, J. W., 1972: Parameterization of the planetary boundary layer for use in general circulation models. *Mon. Wea. Rev.*, **100**, 93–106.

——, 1976: On the entrainment rate of a stratocumulus topped mixed layer. *Quart. J. Roy. Meteor. Soc.*, **102**, 563–582.

——, 1980: Cloud top entrainment instability. *J. Atmos. Sci.*, **37**, 131–147.

——, 1981: On the distribution of mean radiative cooling at the top of a stratocumulus-capped mixed layer. *Quart. J. Roy. Meteor. Soc.*, **107**, 191–202.

Emanuel, K. A., 1981: A similarity theory for unsaturated downdrafts within clouds. *J. Atmos. Sci.* **38**, 1541–1557.

Hanson, H. P., 1984: On mixed layer modeling of the stratocumulus-topped marine boundary layer. *J. Atmos. Sci.*, **41**, 1226–1234.

Kahn, P. H., and J. A. Businger, 1979: The effect of radiative flux divergence on entrainment of a saturated convective boundary layer. *Quart. J. Roy. Meteor. Soc.*, **105**, 303–306.

LaMontagne, R. G., and J. W. Telford, 1983: Cloud top mixing in small cumuli. *J. Atmos. Sci.*, **40**, 2148–2156.

Lilly, D. K., 1968: Models of cloud-topped mixed layers under a strong inversion. *Quart. J. Roy. Meteor. Soc.*, **94**, 292–308.

——, and W. H. Schubert, 1980: The effects of radiative cooling in a cloud-topped mixed layer. *J. Atmos. Sci.*, **37**, 482–487.

Ludlam, F. H., 1966: Cumulus and cumulonimbus convection. *Tellus*, **18**, 687–698.

Moeng, C-H., and A. Arakawa, 1980: A numerical study of a marine subtropical stratus cloud layer and its stability. *J. Atmos. Sci.*, **37**, 2661–2676.

Ogura, Y., and H-R. Cho, 1973: Diagnostic determination of cumulus cloud populations from observed large-scale variables. *J. Atmos. Sci.*, **30**, 1276–1286.

Paluch, I. R., 1979: The entrainment mechanism in Colorado cumuli. *J. Atmos. Sci.*, **36**, 2467–2478.

Randall, D. A., 1980: Conditional instability of the first kind upside-down. *J. Atmos. Sci.*, **37**, 125–130.

Rogers, D. P., J. W. Telford and S. K. Chai, 1985: Entrainment and the temporal development of the microphysics of convective clouds, *J. Atmos. Sci.*, **42**, 1846–1858.

Schubert W. H., 1976: Experiments with Lilly's cloud-topped mixed layer model. *J. Atmos. Sci.*, **33**, 436–446.

Squires, P., 1958: Penetrative downdraft in cumuli. *Tellus*, **10**, 381–389.

Stage, S. A., and J. A. Businger, 1981a: A model for entrainment into a cloud-topped boundary layer. Part I: Model description and application to a cold air outbreak. *J. Atmos. Sci.*, **38**, 2213–2229.

——, and ——, 1981b: A model for entrainment into a cloud-topped boundary layer. Part II: Discussion of model behavior and comparison with other models. *J. Atmos. Sci.*, **38**, 2230–2242.

Suarez, M. J., A. Arakawa and D. A. Randall, 1983: The parameterization of the planetary boundary layer in the UCLA general circulation model: Formulation and results. *Mon. Wea. Rev.*, **111**, 2224–2243.

Telford, J. W., 1975: Turbulence, entrainment, and mixing in cloud dynamics. *Pure. Appl. Geophys.*, **113**, 1067–1084.

——, and P. B. Wagner, 1980: The dynamical and liquid water structure of the small cumulus as determined from its environment. *Pure. Appl. Geophys.*, **118**, 935–952.

Yanai, M., W. Esbenson and J. Chu, 1973: Determination of bulk properties of tropical cloud clusters from large-scale heat and moisture budgets. *J. Atmos. Sci.*, **31**, 1297–1307.